第 36 卷第 3 期
2020 年 3 月

无 机 化 学 学 报
CHINESE JOURNAL OF INORGANIC CHEMISTRY

Vol.36 No.3
536-546

工艺参数对 *o*-$LiMnO_2$ 相纯度及 $Li_{1.6}Mn_{1.6}O_4$ 合成的影响及作用

符雨尧　杨喜云*　黄海强　王园园　李计深
(中南大学冶金与环境学院,长沙　410083)

摘要：以 $MnSO_4$,$KMnO_4$ 及 LiOH 为原料,经水热处理后得到 $LiMnO_2$,再由固相焙烧得到尖晶石相 $Li_{1.6}Mn_{1.6}O_4$,酸洗处理后得到锂离子筛。研究了水热温度,氧气和 MnO_4^-/Mn^{2+}的物质的量之比($n_{MnO_4^-}$:$n_{Mn^{2+}}$)对所得 $LiMnO_2$ 的组成及相应前驱体 $Li_{1.6}Mn_{1.6}O_4$ 酸处理中 Mn 溶损率的影响。开路电势测量及化学分析表明,氧气会参与反应。若按照理论氧化剂用量 $n_{MnO_4^-}$:$n_{Mn^{2+}}$=1:4 进行水热反应会导致杂质 Li_2MnO_3 和 $LiMn_2O_4$ 的生成。若控制水热温度为 160 ℃,$n_{MnO_4^-}$:$n_{Mn^{2+}}$=1:6 时可得到纯相正交 $LiMnO_2$(*o*-$LiMnO_2$)。所得离子筛在高镁锂比盐湖卤水中 Li^+吸附容量可达 42.87 mg·g^{-1},且对 Li^+具有优异的选择吸附性并遵循化学吸附过程。经过 5 个循环后吸附容量保持在 37.21 mg·g^{-1},锰溶损率降至 0.34%。

关键词：水热合成；尖晶石相；离子筛；$Li_{1.6}Mn_{1.6}O_4$；锂吸附
中图分类号：O614.111；O647.3　　**文献标识码**：A　　**文章编号**：1001-4861(2020)03-0536-11
DOI:10.11862/CJIC.2020.038

Role of Process Parameters on Phase Purity of *o*-$LiMnO_2$ and Synthesis of $Li_{1.6}Mn_{1.6}O_4$ as Lithium Ion-Sieve

FU Yu-Yao　YANG Xi-Yun*　HUANG Hai-Qiang　WANG Yuan-Yuan　LI Ji-Shen
(*School of Metallurgy and Environment, Central South University, Changsha* 410083, *China*)

Abstract: Spinel $Li_{1.6}Mn_{1.6}O_4$ was synthesized by hydrothermal oxidation of $MnSO_4$ with $KMnO_4$ to form $LiMnO_2$ following solid-phase roasting. Acid pickling transforms $Li_{1.6}Mn_{1.6}O_4$ to lithium ion-sieve. The effects of hydrothermal temperature, oxygen and molar ratio of MnO_4^- to Mn^{2+} ($n_{MnO_4^-}$:$n_{Mn^{2+}}$) on $LiMnO_2$ composition and the dissolution percentage of manganese from $Li_{1.6}Mn_{1.6}O_4$ during acid pickling were investigated. Open circuit potential measurement and chemical analysis indicate that oxygen in the air has involved in the hydrothermal reaction to produce $LiMnO_2$ accompanied by formation of Li_2MnO_3 and $LiMn_2O_4$ impurities at a theoretical $n_{MnO_4^-}$:$n_{Mn^{2+}}$ of 1:4. Pure orthogonal $LiMnO_2$ (*o*-$LiMnO_2$) was obtained with a molar ratio of MnO_4^- to Mn^{2+} of 1:6 at 160 ℃. The Li^+ adsorption capacity in salt lake brine was 42.87 mg·g^{-1}. The lithium ion-sieve showed excellent adsorption selectivity toward Li^+ in salt lake brine and followed a chemical adsorption process. The adsorption capacity remained at 37.21 mg·g^{-1} and the dissolution percentage of manganese decreased to 0.34% after 5 cycles.

Keywords: hydrothermal synthesis; spinel phase; ion-sieve; $Li_{1.6}Mn_{1.6}O_4$; Li adsorption

Lithium is known as a new energy metal and drives the world forward[1]. The rapid development of new energy vehicles leads to the increasing demand for lithium[2-3]. Lithium are distributed in seawater, salt lake brines and minerals such as spodumene and lepidolite. China has abundant salt lake brines with

收稿日期:2019-09-26。收修改稿日期:2019-11-28。
国家自然科学基金(No.51574286)、中国博士后科学基金(No.2016M592448)和中南大学博士后基金资助项目。
*通信联系人。E-mail:yxy7412@csu.edu.cn

high mass ratios of Mg to Li.

Lithium ion-sieve adsorption is the most promising method of recovering lithium from salt lake brines due to its low cost, no pollution and high selectivity. Manganese oxide-based ion sieve $H_{1.6}Mn_{1.6}O_4$ has the highest theoretical adsorption capacity (68 $mg \cdot g^{-1}$) and attracts most attention. The most common synthesis process of lithium ion-sieve is hydrothermal formation of $LiMnO_2$ followed by roasting and acid pickling. Two types of Mn^{3+} resource were adopted during the hydrothermal synthesis of $LiMnO_2$: One is Mn_2O_3 obtained by roasting electrolytic MnO_2; The other depends on the *in-situ* formation of MnOOH using oxidant and Mn^{2+}-containing solutions[4-10]. The latter is more convenient compared to the former and widely applied for the synthesis of lithium ion-sieve. However, the actual lithium adsorption capacity in salt lake brine was generally lower than 30 $mg \cdot g^{-1}$ and the dissolution percentage of manganese from $Li_{1.6}Mn_{1.6}O_4$ during the acid treatment greater than 3%[11-14], which limits the industrial application. Many scholars focused on the effect of synthesis parameters on the adsorption capacity and stability of lithium ion-sieve. In fact, Mn^{2+} is easy to oxidize by oxygen in the process of *in-situ* formation of MnOOH, which makes the synthesis process carry out in an inert atmosphere[15]. However, keeping an inert atmosphere is inconvenient and high cost. It is seldom reported the effect of oxygen as oxidant on the composition in the process of hydrothermal synthesis of $LiMnO_2$.

In this paper, lithium ion-sieve was synthesized by hydrothermal oxidation of $MnSO_4$ with $KMnO_4$ to form $LiMnO_2$ following solid-phase roasting and acid pickling. The effects of hydrothermal temperature, the molar ratio of MnO_4^- to Mn^{2+} and oxygen in the air on the composition of $LiMnO_2$ were investigated in detail. The adsorption kinetics and separation performance of lithium ion sieve in salt lake brine have been discussed.

1 Experimental

1.1 Materials and reagents

$LiOH \cdot H_2O$, $KMnO_4$ and $MnSO_4$ produced by Sinopharm Chemical Reagent Co., Ltd. were used as raw materials, and all reagents were of analytical grade. Salt lake brine was from the Lop Nor salt lake and its main composition was listed in Table 1.

Table 1　Composition of salt lake brine

$mg \cdot L^{-1}$

Mg	Na	K	Li	Ca	S	B	Si
106 100	5 020	2 480	220.2	27.24	6 831	519.0	28.05
P	Mo	Fe	As	Co	Ga	Cu	V
5.26	4.50	0.87	0.63	0.53	0.45	0.42	0.32
Mn	Sn	Cr	Al	Ni	Pb	Y	Cd
0.28	0.23	0.20	0.13	0.12	0.04	0.04	0.03

1.2 Pretreatment process

$MnSO_4$ solution and $KMnO_4$ solution were simultaneously added into a LiOH solution through a flowmeter. The mixed solution volume was kept around 500 mL and molar ratio of Li to Mn fixed as 4.5. After mechanically stirring for 2 h, the mixture was transferred into a 1.0 L autoclave.

1.3 Preparation of $LiMnO_2$ and precursor $Li_{1.6}Mn_{1.6}O_4$

$LiMnO_2$ precipitate was obtained by hydrothermal treating the above mixture for 18 h at a certain temperature. After filtration and washing several times with deionized water, the resulting $LiMnO_2$ was calcined in a muffle furnace at 350~500 ℃ for 4 h to form the precursor of lithium ion-sieve $Li_{1.6}Mn_{1.6}O_4$.

1.4 Preparation of lithium ion-sieve

The precursor (0.6 g) was added to 100 mL of 0.5 $mol \cdot L^{-1}$ HCl at 30 ℃ and stirred for 3 hours, centrifuged, washed, and dried to obtain lithium ion sieve. The percentage of dissolved manganese and extraction percentage of Li^+ from each precursor during acid treatment were calculated by the following equa

tion:

$$R_i=\frac{c_i v_1}{m_s w_i} \quad (1)$$

where R_i is the rate of dissolved metal ions, %; c_i is the concentration of metal ions in the supernatant ($mg\cdot L^{-1}$); v_1 is the volume of the solution (L); m_s is the mass of the precursor (mg); w_i is the mass fraction of metal in the precursor (%).

1.5 Adsorption properties of lithium ion-sieve

The lithium ion-sieve (0.30 g) was immersed in 100 mL salt lake brine and stirred at 30 ℃ for 20 h. Then the suspension was filtered and the concentrations of all the metal ions in the supernatant were determined. The adsorption capacity or the amount of metal ion adsorbed per gram of ion sieve at equilibrium (Q_e), distribution coefficient (K_d), and separation factor (α_{Me}^{Li}) were calculated using equations (**2~4**):

$$Q_t=\frac{v_2(c_0-c_t)}{m_0} \quad (2)$$

$$K_d=\frac{c_0-c_t}{m_0 c_t} \quad (3)$$

$$\alpha_{Me}^{Li}=\frac{k_d(Li)}{k_d(Me)} \quad (4)$$

where Q_t represents the adsorption capacity of Li^+ ($mg\cdot g^{-1}$), c_0 is the concentration of Li^+ in the salt lake brine ($mg\cdot L^{-1}$), c_t is the concentration of Li^+ in the filtrate after adsorption ($mg\cdot L^{-1}$), v_2 is the volume of salt lake brine (L), m_0 is the mass of lithium ion-sieve (g); K_d represents the distribution coefficient of metal ion Me^{n+} in brine, and α_{Me}^{Li} is a separation coefficient between lithium and Me (Na^+, K^+, Mg^{2+}) in the adsorption process.

1.6 Adsorption kinetics

The lithium ion-sieve (0.30 g) was added to 100 mL of salt lake brine and stirred at 25 ℃, samples were taken at 1, 2, 6, 12, 20 and 30 h respectively to determine the concentration of Li^+ in the supernatant to calculate the adsorption capacity of lithium ion sieve. The adsorption process of lithium ion sieve was simulated by pseudo-second-order kinetic model and pseudo-first-order kinetic model, respectively.

1.7 Circulating property of lithium ion sieve

The desorption and adsorption of Li^+ have been repeated 5 times to test the recycling performance of the lithium ion sieve. In each desorption process, the precursor $Li_{1.6}Mn_{1.6}O_4$ were immersed into 0.5 $mol\cdot L^{-1}$ HCl solution. The ratio of solid to liquid was controlled at 1/100 (w/V, $g\cdot mL^{-1}$). After acid pickling at 30 ℃ for 4 h, the lithium ion-sieve was filtered, washed and dried. Then the ion sieve was added into the salt lake brine to adsorb lithium. The above operations were termed as one cycle. The concentrations of manganese and lithium in the effluents were analyzed to calculate the dissolution percentage of manganese and adsorption capacity of lithium of each cycle. The percentage of dissolved manganese and the capacity of lithium adsorption of each cycle were calculated by the equation (**1**) and the equation (**2**), respectively.

1.8 Characterization and chemical analysis

The crystalline phases were characterized by XRD using a Rigaku Rint-2000 X-ray diffractometer equipped with monochromatized Cu $K\alpha$ radiation (λ= 0.154 056 nm), operating at 40 kV and 100 mA, and a scanning rate of $10°\cdot min^{-1}$ in a 2θ range of 10°~80°. The morphology of the particles was characterized by field emission scanning electron microscopy (MIRA3 TESCAN). The concentrations of manganese and lithium were determined using an atomic absorption spectrophotometer (TAS-999F, Beijing). The manganese valence was characterized after oxidation-reduction titration analyses by using the standard oxalic acid method[16].

DTA-TG curve was performed on a MAC science thermal analyzer (system 001 200 TG-DTA) at a heating rate of 5 $℃\cdot min^{-1}$ under an air atmosphere. Open circuit measurement was carried out using a Reference 600 + electrochemical workstation. The working electrode was Pt wire (0.5 mm diameter, 0.5 cm long). The counter electrode was a platinum foil (about 2 cm^2). All potentials were measured and reported relative to a saturated Hg/HgO electrode.

When the $MnSO_4$ and $KMnO_4$ solution were added into the LiOH solution, the change of open circuit potential with time was recorded.

2 Results and discussion

2.1 Effect of hydrothermal temperature

The XRD patterns of $LiMnO_2$ obtained at different hydrothermal temperatures are shown in Fig.1. Table 2 shows the extraction percentage of Li^+ and the percentage of dissolved manganese of the precursor as well as the adsorption capacity of Li^+ of the corresponding lithium ion sieve.

It is found from Fig.1 that all the XRD patterns are indexed to orthogonal $LiMnO_2$ (PDF No.35-0749). A characteristic impurity peak near 18.7° was observed. A lot of scholars have different opinions about the peak source. Wang et al ascribed the peak to MnO_2 due to $Mn(OH)_2$ oxidation[17]. Ji et al. and Liu et al. attributed it to Li_2MnO_3 owing to the oxidation of Mn^{3+} to Mn^{4+} by oxygen from the autoclave[18-19]. Increasing hydrothermal temperature lead to an increase of peak intensity at 18.7°. Supposing that oxygen participates in the reaction to some extent during the pretreatment process and hydrothermal reaction. The impurity peak at 18.7° was attributed to Li_2MnO_3 and $LiMn_2O_4$. The exact origin of the peak was discussed in the following section.

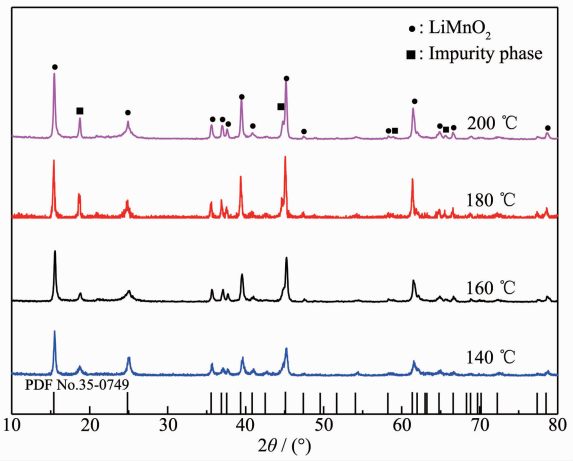

Fig.1　XRD patterns of precipitates obtained at different hydrothermal temperatures

To check the effect of hydrothermal temperature on the composition of precursor $Li_{1.6}Mn_{1.6}O_4$, $LiMnO_2$ was roasted at 450 ℃ for 4 h. Table 2 shows the properties of precursor and adsorption capacity of its ion-sieve $H_{1.6}Mn_{1.6}O_4$. It is observed that the percentage of dissolved manganese increased with increasing hydrothermal temperature. Both the extraction percentage of Li^+ and adsorption capacity increase slightly with the increasing temperature, reaching a maximum at 160 ℃, and then decreased. The increase in the percentage of dissolved manganese is due to an increase in $LiMn_2O_4$ content. The extraction percentage of Li^+ is related to the crystal structure of $LiMnO_2$. When the hydrothermal temperature reached 140 ℃, the reaction rate became slow and $LiMnO_2$ growth was imperfect, resulting in a low extraction percentage of Li^+ and adsorption capacity. When the temperature increased to 160 ℃, $LiMnO_2$ crystal develops completely, which is beneficial to the extraction and adsorption of Li^+ ions. Further increasing the temperature leads to the formation of Li_2MnO_3, which in turn reduced Li^+ extraction and adsorption performance[20].

Table 2　Performance of precursor and ion-sieve synthesized at different hydrothermal temperatures

Temperature / ℃	Dissolution percentage of manganese / %	Extraction percentage of Li^+ / %	Adsorption capacity of Li^+ / (mg·g^{-1})
140	2.44	84.88	28.35
160	2.62	86.32	30.29
180	2.74	84.62	26.56
200	2.93	85.03	26.46

2.2 Effect of molar ratio of MnO_4^-/Mn^{2+}

The formation of orthogonal $LiMnO_2$ can be expressed by equation (**5**). The theoretical molar ratio of MnO_4^- to Mn^{2+} was 1∶4. However, the presence of either Li_2MnO_3 or $LiMn_2O_4$ as shown in Fig.1 indicates that the oxidant was excessive in the hydrothermal reaction. It is assumed that the excessive oxidant originates from oxygen in the air and autoclave.

To support the assumption, the pretreatment process was carried out in a glove box to completely

isolate the oxygen and the molar ratio of MnO_4^-/Mn^{2+} was kept at 1:4. After the pretreatment was completed, the suspension was transferred into the autoclave and N_2 was blown for 30 min. The XRD patterns of the resulting hydrothermal products with and without oxygen isolation are shown in Fig.2.

$$MnO_4^- + 4Mn^{2+} + 12OH^- + 5Li^+ \rightarrow 5LiMnO_2 + 6H_2O \quad (5)$$

It can be seen from Fig.2 that the hydrothermal product is pure $LiMnO_2$ (PDF No.35-0749) after oxygen was completely isolated. The manganese content was 58.42%, nearly identical to the theoretical content (58.52%) of $LiMnO_2$, and manganese valence was 3.08. This result indicates that oxygen in the air dissolves into the suspension in the pretreatment process and participates in the oxidation reaction.

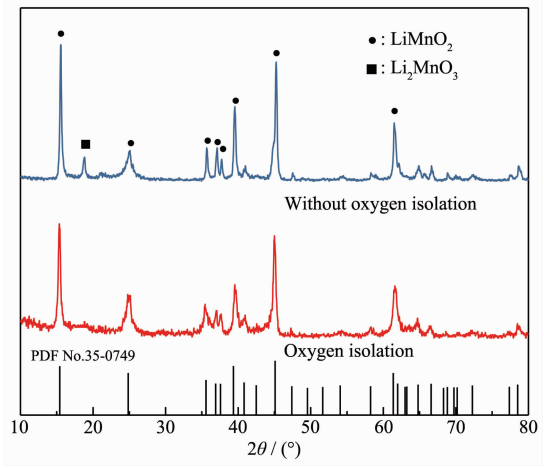

Fig.2 XRD patterns of hydrothermal product obtained after complete oxygen isolation

In order to avoid the inconvenience of oxygen removal, an attempt to reduce the amount of oxidant $KMnO_4$ was made by changing the $n_{MnO_4^-}:n_{Mn^{2+}}$ from 1:4 to 1:5, 1:5.5 even 1:6, the XRD patterns of the resulting precipitates are shown in Fig.3.

As shown in Fig.3, the impurity peak at 18.7° was significantly reduced and even disappeared at a the $n_{MnO_4^-}:n_{Mn^{2+}}$ of 1:6. The results again confirm the fact that oxygen either from air or autoclave participates in the oxidation reaction.

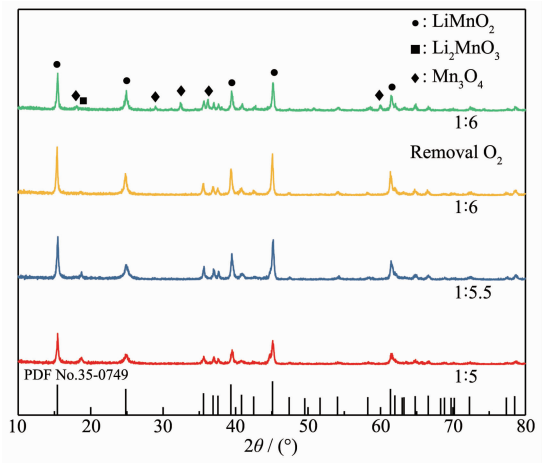

Fig.3 XRD patterns of hydrothermal products obtained under different molar ratios of $n_{MnO_4^-}:n_{Mn^{2+}}$

To further support the fact, the molar ratio of MnO_4^- to Mn^{2+} was kept at 1:6, and N_2 continuously blown into the autoclave for 30 min in order to remove the oxygen in the autoclave and suspension. The XRD patterns of the hydrothermal products are also shown in Fig.3. Both $LiMnO_2$ and Mn_3O_4 diffraction peaks were observed. The appearance of Mn_3O_4 indicates that the oxidation reaction was incomplete in the absence of oxygen when the molar ratio of MnO_4^- to Mn^{2+} was 1:6.

The valence of Mn (Z_{Mn}) and mass fraction of manganese (w_{Mn}) in the $LiMnO_2$ sample obtained at different molar ratios of MnO_4^- to Mn^{2+} were measured. The results are shown in Table 3.

When the molar ratio of MnO_4^- to Mn^{2+} decreased from 1:4 to 1:6, the Mn valence decreased from 3.32 to 3.02 and the mass fraction of manganese increased from 55.69% to 58.54%. The valence of Mn higher than 3.0 means that the sample contains other compounds besides $LiMnO_2$. The theoretical mass fraction of manganese in Li_2MnO_3, $LiMnO_2$, $LiMn_2O_4$ and Mn_3O_4 is 47.03%, 58.52%, 60.77% and 72.03%, respectively. The sample obtained at a molar ratio of

Table 3 Mn valence in $LiMnO_2$ at different molar ratios of MnO_4^- to Mn^{2+}

$n_{MnO_4^-}:n_{Mn^{2+}}$	1:4	1:5	1:5.5	1:6	1:6 (O_2 removal)
w_{Mn} / %	55.69	56.62	57.61	58.54	58.70
Z_{Mn}	3.32	3.23	3.15	3.02	3.00

MnO_4^- to Mn^{2+} of 1:6 had a mass fraction of manganese close to $LiMnO_2$. When the oxygen in the autoclave was removed, a small amount of Mn_3O_4 was formed due to insufficient oxidation, resulting in a higher mass percentage of manganese.

It is deduced from the mass fraction of manganese and valence in Table 3 that the sample is composed of $LiMnO_2$, Li_2MnO_3 and $LiMn_2O_4$. Assuming that the total mass of Mn was 1 mol, $LiMnO_2$, Li_2MnO_3 and $LiMn_2O_4$ account for x, y and $(1-x-y)$ mol, respectively. The mass fraction of $LiMnO_2$ (w_{LiMnO_2}), Li_2MnO_3 ($w_{Li_2MnO_3}$) and $LiMn_2O_4$ ($w_{LiMn_2O_4}$) in the sample can be calculated by the following equation (**6~10**). The results are shown in Table 4.

$$3x+4y+3.5(1-x-y)=Z_{Mn} \quad (6)$$

$$\frac{x}{58.52\%}+\frac{y}{47.03\%}+\frac{1-x-y}{60.77\%}=\frac{1}{w_{Mn}} \quad (7)$$

$$\omega_{LiMnO_2}=\frac{xw_{Mn}M_{LiMnO_2}}{M_{Mn}}\times 100\% \quad (8)$$

$$\omega_{Li_2MnO_3}=\frac{yw_{Mn}M_{Li_2MnO_3}}{M_{Mn}}\times 100\% \quad (9)$$

$$\omega_{LiMn_2O_4}=[1-(w_{LiMnO_2}+w_{Li_2MnO_3})]\times 100\% \quad (10)$$

Where M_{LiMnO_2}, $M_{Li_2MnO_3}$ and M_{Mn} represent the molecular weight of $LiMnO_2$, Li_2MnO_3 and the relative atomic weight of manganese, respectively.

It can be seen from Table 4 that $LiMnO_2$ content increased from 56.54% to 98.16% while Li_2MnO_3 decreased from 27.72% to 0.16% when the molar ratio of MnO_4^- to Mn^{2+} changed from 1:4 to 1:6. When the MnO_4^-/Mn^{2+} ratio decreased to 1:6, the product was nearly pure $LiMnO_2$ with a very small amount of Li_2MnO_3 and $LiMn_2O_4$. It is deduced that pure $LiMnO_2$ can be obtained when the amount of oxidant was reduced to a certain extent.

In order to find the effect of oxygen on the pretreatment process, the change of open circuit potential with pretreatment time was recorded and is shown in Fig.4. Before the MnO_4^- and Mn^{2+} solutions were added into the LiOH solution, the open circuit potential maintained constant with time. When MnO_4^- and Mn^{2+} were added dropwise into the LiOH solution, redox reaction occurs and forms MnOOH through equation (**11**) and (**12**).

$$5H^+ + MnO_4^- + 4e \rightarrow MnOOH + 2H_2O \quad (11)$$

$$12OH^- + 4Mn^{2+} - 4e \rightarrow 4MnOOH + 4H_2O \quad (12)$$

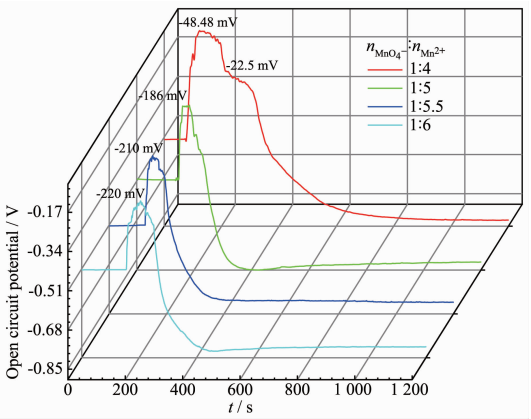

Fig.4　Open circuit potential with time during pretreatment

According to the Nernst equation, the open circuit potential depends on the concentration ratio of MnO_4^- to Mn^{2+} in the solution, increasing with increasing concentration of MnO_4^-, and decreasing with increasing concentration of Mn^{2+}. Upon MnO_4^- and Mn^{2+} solutions were added into the LiOH solution, the $MnSO_4$ solution immediately formed $Mn(OH)_2$ precipitate instead of oxidation to form MnOOH, resulting in the increase of open circuit potential. After a period of time, MnO_4^- and Mn^{2+} ions form MnOOH and the concentration of MnO_4^- decreased, resulting in a sharp drop in the open circuit potential. When the addition rate was equal to the oxidation reaction rate, the concentrations of MnO_4^- and Mn^{2+} remained unchanged and the open circuit potential kept stable.

Table 4　Hydrothermal product components obtained at different molar ratios of MnO_4^- to Mn^{2+}

$n_{MnO_4^-}$:$n_{Mn^{2+}}$	w_{LiMnO_2} / %	$w_{Li_2MnO_3}$ / %	$w_{LiMn_2O_4}$ / %
1:4	56.54	27.72	15.74
1:5	67.62	19.13	13.25
1:5.5	77.23	10.35	12.42
1:6	98.16	0.16	1.68

When the molar ratio of MnO_4^- to Mn^{2+} changed from 1∶4 to 1∶6, the maximum open circuit potential decreases from −48.4 to −220 mV due to the decreasing of MnO_4^- concentration. However, the stable open circuit potentials were very close. The results again support the fact that oxygen from the air acts as an oxidant and participates in the oxidation. When the molar ratio of MnO_4^- to Mn^{2+} was high, such as 1∶4 or 1∶5, excessive oxidant resulted in the oxidation of MnOOH to Mn^{4+} and subsequent formation of Li_2MnO_3 and $LiMn_2O_4$. When the molar ratio of MnO_4^- to Mn^{2+} was relatively low, MnO_4^- combined with oxygen oxidizes all Mn^{2+} ions to produce pure MnOOH followed by conversion to $LiMnO_2$. As a result, all MnO_4^- and Mn^{2+} ions were transformed to precipitate and made no great difference to the open circuit potential.

It is deduced that the $LiMnO_2$ formation reaction proceeds according to equation (**13**).

$$MnO_4^- + 6Mn^{2+} + 18OH^- + 7Li^+ + 0.5O_2 \rightarrow 7LiMnO_2 + 9H_2O \quad (\mathbf{13})$$

It is calculated that the oxygen from the autoclave only accounts for 23.44% of the theoretical oxygen amount, the other 76.56% is from the dissolved oxygen during the pretreatment process.

Fig.5 shows the XRD patterns of $Li_{1.6}Mn_{1.6}O_4$ obtained under different molar ratios of $n_{MnO_4^-}$∶$n_{Mn^{2+}}$. It is shown that all the XRD patterns are indexed to $Li_{1.6}Mn_{1.6}O_4$ (PDF No.52-1841). A small impurity peak near 20.96° was observed in the range of 1∶4, 1∶5 and 1∶5.5. When the molar radio of MnO_4^- to Mn^{2+} was 1∶6, the impurity peak disappeared. In addition, the peak intensity ratio of (400) to(311) plane gradually increased from 1.64 to 2.27 when the molar ratio of MnO_4^- to Mn^{2+} increased from 1∶6 to 1∶4. Increasing the lithium content in the spinel may lead to growth rate of (400)-plane in the lattice being faster than (311) plane. The structure tend to be regular octahedron[21]. When molar ratio of MnO_4^- to Mn^{2+} was 1∶6, the peak intensity ratio of (400) to (311) was 1.64, close to the theoretical ratio (1.61) denoted by the PDF No.52-1841. This result indicates that reducing $KMnO_4$ amount can obtain the desirable phase and structure.

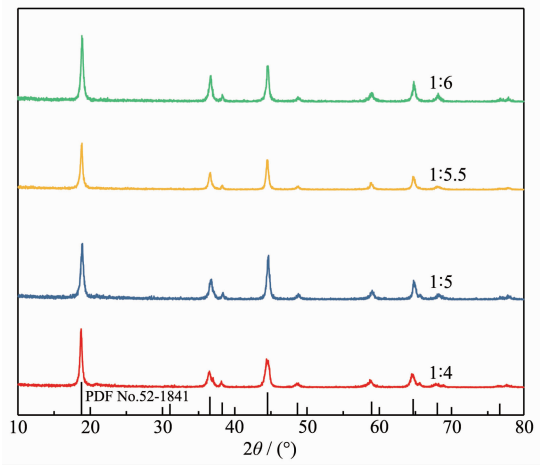

Fig.5 XRD patterns of $Li_{1.6}Mn_{1.6}O_4$ obtained under different molar ratios of $n_{MnO_4^-}$∶$n_{Mn^{2+}}$

Fig.6 shows the SEM images of $Li_{1.6}Mn_{1.6}O_4$, lithium-extracted and lithium-reinserted sample. The morphology did not change significantly, the sizes of most particles were in a range of 0.1~0.2 μm, which was small enough and beneficial for ionic diffusion. However, the aggregate phenomenon was reduced after pickling. The looser surface reduces the mass transfer resistance and completes the ion exchange process

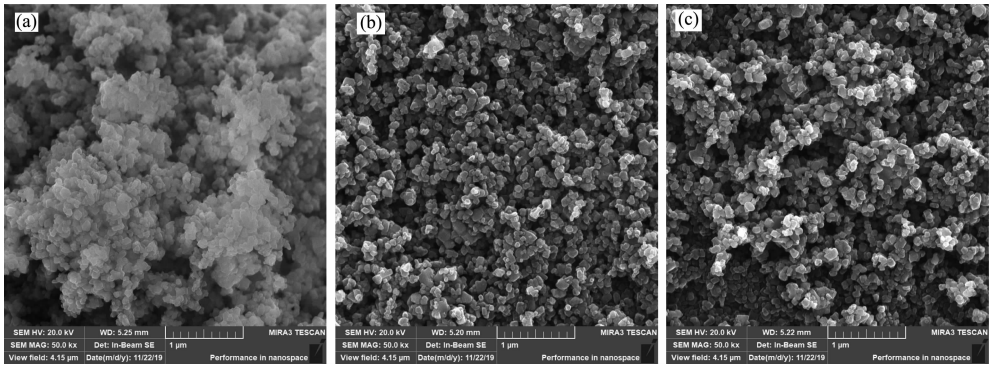

Fig.6 SEM images of $Li_{1.6}Mn_{1.6}O_4$ (a), lithium-extracted (b) and lithium-reinserted sample (c) obtained under molar radio of MnO_4^- to Mn^{2+} of 1∶6

quickly.

Table 5 shows the properties of $Li_{1.6}Mn_{1.6}O_4$ obtained under different molar ratios of $n_{MnO_4^-}$:$n_{Mn^{2+}}$ and the adsorption capacity of the corresponding lithium ion-sieve.

As can be seen from Table 5, a lower molar ratio lead to a higher adsorption capacity due to smaller amounts of impurities as shown in Table 4. The percentage of dissolved manganese showed a small decrease due to the decrease of $LiMn_2O_4$ content. It is found that the adsorption capacity of Li^+ and the extraction percentage of Li^+ increased with an increase of mass fraction of $LiMnO_2$.

Table 5　Performance of precursor and ion-sieve obtained under different molar ratios of MnO_4^-/Mn^{2+}

$n_{MnO_4^-}$:$n_{Mn^{2+}}$	w_{LiMnO_2} / %	Extraction percentage of Li^+ /%	Dissolution percentage of manganese /%	Adsorption capacity of Li^+ / (mg·g^{-1})
1:4	55.85	86.32	2.62	30.29
1:5	66.70	93.77	2.51	37.80
1:5.5	77.23	95.48	2.42	39.43
1:6	98.16	97.82	2.18	42.87

2.3　Effect of roasting temperature

DTA-TG (differential thermal-gravimetric analysis) curve was measured to find the optimum roasting temperature of o-$LiMnO_2$ obtained at a $n_{MnO_4^-}$:$n_{Mn^{2+}}$ of 1:6. As shown in Fig.7, the evaporation of adsorbed water caused nearly 1% weight loss below 200 ℃. When the temperature was in a range from 200 to 480 ℃, $LiMnO_2$ oxidation occurd through equation **14** and lead to 5.2% weight gain. A weight loss about 0.26% was observed for the temperature between 349 and 390 ℃, which may result from the transformation of Li_2MnO_3 and $LiMn_2O_4$ to $LiMnO_2$ accompanied by oxygen release according to reaction (**15**)[22].

$$8LiMnO_2+2O_2 \rightarrow 5Li_{1.6}Mn_{1.6}O_4 \quad (\mathbf{14})$$

$$Li_2MnO_3+LiMn_2O_4 \rightarrow 3LiMnO_2+0.5O_2 \quad (\mathbf{15})$$

The continuous decrease in weight above 480 ℃ was due to the decomposition of $Li_{1.6}Mn_{1.6}O_4$ and the volatilization of Li^+[23].

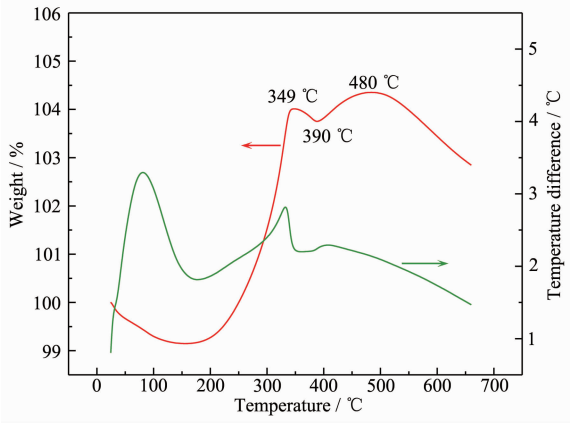

Air atmosphere and heating rate of 5 ℃·min^{-1}

Fig.7　DTA-TG curves of $LiMnO_2$

The XRD patterns of $Li_{1.6}Mn_{1.6}O_4$ obtained at different roasting temperatures are shown in Fig.8.

It can be seen from Fig.8 that pure $Li_{1.6}Mn_{1.6}O_4$ was obtained by roasting $LiMnO_2$ at 350~450 ℃ for 4 h. The higher the roasting temperature, the better the crystallinity was. When the temperature reaches 500 ℃, some peaks appear at 20.6° and 65.6° and are more likely to be characteristic peaks of Li_2MnO_3 and $LiMn_2O_4$[13].

Fig.9 shows the extraction percentage of Li^+ and the percentage of dissolved manganese of the precursor as well as the adsorption capacity of Li^+ of the corresponding lithium ion sieve at different roasting

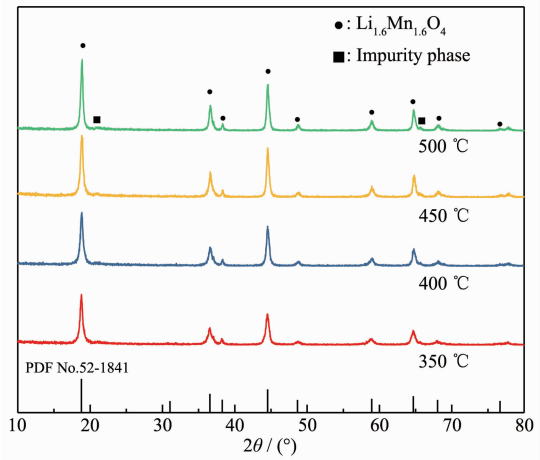

Fig.8　XRD patterns of samples at different roasting temperatures

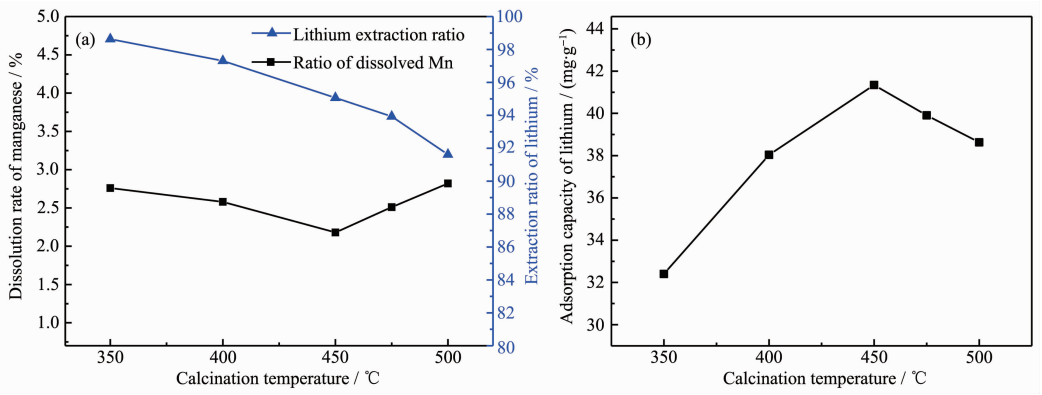

Fig.9 Extraction percentage of Li^+ and dissolution percentage of manganese (a) and corresponding adsorption capacity of Li^+ (b) at different roasting temperatures

temperatures. It is observed that the extraction percentage of Li^+ gradually decreased with an increase of roasting temperature. The percentage of dissolved manganese showed a similar trend but appeared a minimum at 450 ℃. The response can be interpreted from two sides. On the one hand, the extraction rate of Li^+ was ion exchange between Li^+ and H^+ ions. As the roasting temperature increased, the $Li_{1.6}Mn_{1.6}O_4$ crystallinity was well developed and lithium ions were more difficult to escape from the crystal lattice[24]. On the other hand, Li_2MnO_3 content increased with increasing temperature, while Li_2MnO_3 did not have Li^+ extraction property in dilute hydrochloric acid. The increase in temperature lead to a more complete oxidation reaction, which in turn decreased the dissolution percentage of manganese. When the temperature exceeded 450 ℃, the sample began to decompose and form Mn^{3+}, resulting in an increase in the dissolution rate of manganese.

The adsorption capacity of Li^+ increased with increasing temperature, reaching a maximum of 41.34 mg·g^{-1} at 450 ℃. After that, it began to decrease. The crystal structure was not well developed at a low temperature. Correspondingly, the adsorption capacity of Li^+ was low. When the temperature exceeded 450 ℃, as shown in Fig.6, the decomposition occured accompanied by Li^+ volatilization[22], resulting in the decrease of adsorption capacity of Li^+.

2.4 Adsorption kinetics, selective adsorption and cycling performance

Fig.10 shows the relationship between the adsorption capacity and time. It is obvious that the adsorption capacity initially increased and then tended to reach equilibrium around 42.76 mg·g^{-1} at 20 h.

The pseudo-first-order kinetic model (equation (**16**)) and the pseudo-second-order kinetic model (equation (**17**)) are used to analyze the adsorption process and determine the rate constant of the adsorption process[24].

$$\lg(Q_e-Q_t)=\lg Q_e-\frac{tk_1}{2.303} \quad (\mathbf{16})$$

$$\frac{t}{Q_t}=\frac{1}{k_2Q_e^2}+\frac{t}{Q_e} \quad (\mathbf{17})$$

$$Q_t=Q_e(1-e^{-k_1t}) \quad (\mathbf{18})$$

where Q_t is adsorption capacity of Li^+ on ion sieve at adsorption time t, mg·g^{-1}; Q_e is equilibrium adsorption capacity of Li^+ on ion sieve, mg·g^{-1}; k_1 is adsorption rate constant of pseudo-first-order kinetic model, h^{-1}; k_2 is adsorption rate constant of pseudo-second-order kinetic model, g·mg^{-1}·h^{-1}; t is adsorption time, h.

The pseudo-first-order kinetic model can be transformed into equation (**18**) and then fitted expo-

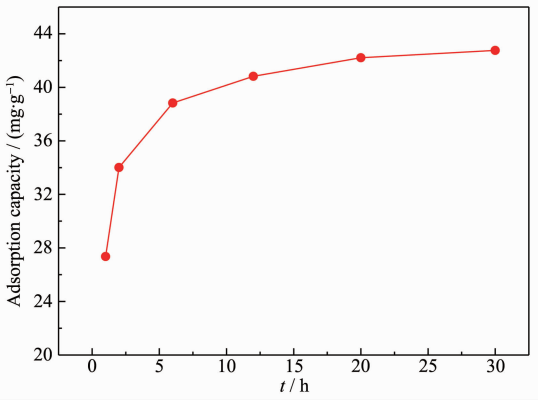

Fig.10 Adsorption capacity aftert different adsorption times

nentially. The kinetic fitting results are shown in Fig. 11. Table 6 lists the fitted parameters.

The correlation coefficient (R^2) of the pseudo-second-order kinetic model for the adsorption process was 0.999, while that of pseudo-first-order kinetic model was 0.909. The result suggests that the adsorption process conformed to the pseudo-second-order kinetic model and was controlled by chemical adsorption process[25-27].

The equilibrium adsorption capacity (Q_e) obtained by fitting pseudo-second-order kinetic model was 43.60 mg·g^{-1}, which was consistent with the maximum adsorption capacity in Fig.10.

Table 7 shows the concentration changes of the main metal ions in the salt lake brine before and after adsorption. Only K^+ ions are adsorbed slightly in salt lake brine, and α_K^{Li} was 33.38, much larger than that for Li^+. Indicating that the lithium ion-sieve towards Li^+ ions had good separation and selectivity performance.

The cycle performance of lithium ion-sieve is shown in Fig.12. The initial adsorption capacity of Li^+ was 42.87 mg·g^{-1} and reduced to 37.21 mg·g^{-1} after five cycles. The dissolution percentage of manganese decreased from 2.33% to 0.34% and remained stable after 3 cycles.

The manganese valence increased from 3.94 to 3.97 after one-cycle acid pickling, indicating that a small amount of Mn^{3+} was present in the precursor and disproportionation occured to form Mn^{4+} and Mn^{2+}. Mn^{2+} entering into the acid solution lead to manganese dissolution. After 2 cycles, the percentage of dissolved manganese tended to be stable, indicating that Mn^{3+} ions had nearly depleted and subsequent manganese dissolution was due to the reduction of $MnO_2·0.5H_2O$ by chloride ions according to equation (**19**).

$$MnO_2·0.5H_2O+4HCl \rightarrow MnCl_2+Cl_2+2.5H_2O \quad (19)$$

The relatively high Li^+ ion adsorption capacity and selectivity prove that the synthesized lithium ion-sieve is an excellent candidate for Li^+ recovery from salt lake brines.

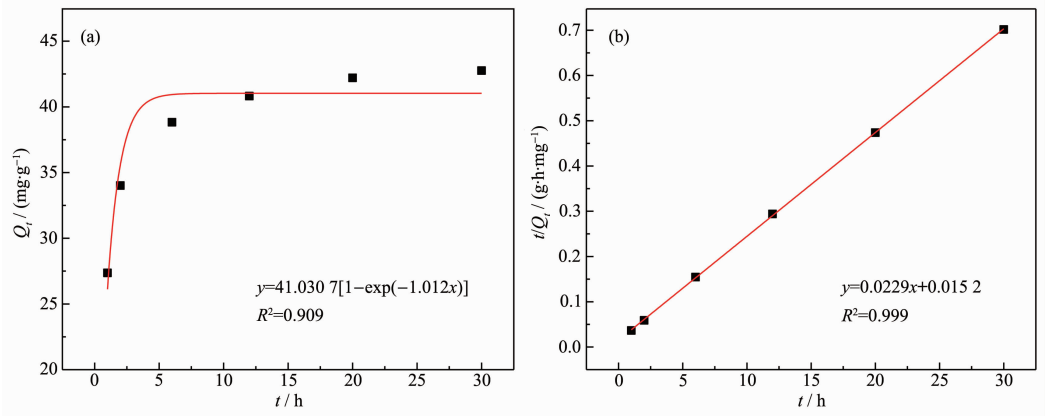

Fig.11　Pseudo-first-order kinetic (a) and pseudo-second-order kinetic curves (b) fitting of ion sieve adsorption

Table 6　Fitting parameters of two kinetic equations

	k_1 / h	k_2 / (g·mg^{-1}·h^{-1})	R^2	Q_e / (mg·g^{-1})
Pseudo-first-order	1.01	—	0.909	41.03
Pseudo-second-order	—	0.035	0.999	43.60

Table 7　Selective adsorption of the ion sieve in salt lake brine

Metal ion	c_0 / (mg·L^{-1})	c_t / (mg·L^{-1})	K_d	α_{Me}^{Li}
Li^+	290	161	0.267	1.0
Na^+	3 020	3 016	0	—
K^+	1 690	1 647	0.008	33.38
Mg^{2+}	109 820	109 815	0	—

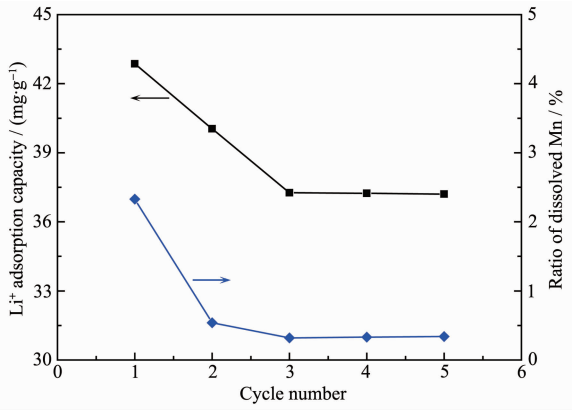

Fig.12 Cycle performance of lithium ion-sieve in salt lake brine

3 Conclusions

$Li_{1.6}Mn_{1.6}O_4$ was synthesized through a hydrothermal reaction to form $LiMnO_2$ followed by roasting. Acid pickling transforms $Li_{1.6}Mn_{1.6}O_4$ to lithium ion-sieve. The results show that hydrothermal temperature, molar ratio of MnO_4^-/Mn^{2+} have a great influence on $LiMnO_2$ purity and adsorption performance of the lithium ion sieve. The $LiMnO_2$ contained a small amount of Li_2MnO_3 and $LiMn_2O_4$. With the presence of oxygen in pretreatment process or hydrothermal reaction, pure orthogonal $LiMnO_2$ was obtained at a molar ratio of MnO_4^- to Mn^{2+} of 1∶6, deviated from the theoretical ratio of 1∶4. Open circuit potential measurement confirms that oxygen participates in the oxidation reaction to form $LiMnO_2$.

Pure $Li_{1.6}Mn_{1.6}O_4$ can be obtained by roasting pure $LiMnO_2$ at 450 ℃ for 4 h. The percentage of dissolved manganese was only 2.18% and the extraction percentage of Li^+ was 97.82%. The adsorption capacity of corresponding lithium ion-sieve in Lop Nor salt lake brine was 42.87 $mg\cdot g^{-1}$. Distribution coefficients of metal ions are in the order: $Li^+ \gg K^+ > Na^+ > Mg^{2+}$. After 5 cycles, the Li^+ ion adsorption capacity was 37.21 $mg\cdot g^{-1}$ and the percentage of dissolved manganese decreased to 0.34% . The adsorption process for the ion-sieve in salt lake brine fits well with a quasi-second-order kinetic model and is controlled by chemical adsorption.

References:

[1] FENG Guo-Fu(封国富), ZHANG Xiao(张骁). *Chinese Journal of Rare Metals*(稀有金属), **2003**,**27**(1):57-61

[2] Ebensperger A, Maxwell P, Moscoso C. *Resour. Policy*, **2005**, **30**(3):218-231

[3] Scrosati B, Garche J. *J. Power Sources*, **2010**,**195**(9):2419-2430

[4] Banov B, Momchilov A, Trifonova A, et al. *J. Power Sources*, **1999**,**81/82**:562-565

[5] Xu H, Sun J, Gao L. *Ionics*, **2013**,**19**(1):63-69

[6] Li K Y, Shua F F, Zhang J W, et al. *Ceram. Int.*, **2015**,**41**(5): 6729-6733

[7] Li X H, Su Z, Wang Y B. *J. Alloys Compd.*, **2018**,**735**:2182-2189

[8] Zhang Q H, Li S P, Sun S Y, et al. *Chem. Eng. Sci.*, **2010**,**65** (1):169-173

[9] Xie J L, Huang X, Zhu Z B, et al. *Ceram. Int.*, **2011**,**37**(1): 419-421

[10]Zhao H Y, Chen B, Cheng C, et al. *Ceram. Int.*, **2015**,**41** (10):15266-15271

[11]Chitrakar R, Kanoh H, Miyai Y, et al. *Chem. Mater.*, **2000**, **12**(10):3151-3157

[12]Chitrakar R, Kanoh H, Miyai Y, et al. *Ind. Eng. Chem. Res.*, **2001**,**40**(9):2054-2058

[13]Xiao J L, Sun S Y, Wang J, et al. *Ind. Eng. Chem. Res.*, **2013**,**52**(34):11967-11973

[14]Shi X C, Zhou D F, Zhang Z B, et al. *Hydrometallurgy*, **2011**,**110**(1/2/3/4):99-106

[15]Sun S Y, Xiao J L, Wang J, et al. *Ind. Eng. Chem. Res.*, **2014**,**53**(40):15517-15521

[16]Gao A L, Sun Z H, Li S P, et al. *Dalton Trans.*, **2018**,**47** (11):3864-3871

[17]WANG Lu(王禄), MA Wei(马伟), HAN Mei(韩梅), et al. *Acta Chim. Sin.*(化学学报), **2007**,**65**(12):1135-1139

[18]Ji H M, Yang G, Miao X W, et al. *Electrochim. Acta*, **2010**, **55**(9):3392-3397

[19]Liu Q, Li Y X, Hu Z L, et al. *Electrochim. Acta*, **2008**,**53** (24):7298-7302

[20]Wang L, Ma W, Liu R, et al. *Solid State Ionics*, **2006**,**177** (17/18):1421-1428

[21]Chitrakar R, Kanoh H, Kim Y S, et al. *J. Solid State Chem.*, **2001**,**160**(1):69-76

[22]Chitrakar R, Sakane K, Umeno A, et al. *J. Solid State Chem.*, **2002**,**169**(1):66-74

[23]Seo H, Na S, Lee B, et al. *J. Ind. Eng. Chem.*, **2018**,**64**:311-317

[24]MA Li-Wen(马立文), CHEN Bai-Zhen(陈白珍), SHI Xi-Chang(石西昌), et al. *Chinese J. Inorg. Chem.*(无机化学学报), **2011**,**27**(4):697-703

[25]Langmuir I. *J. Am. Chem. Soc.*, **1918**,**40**(9):1361-1403

[26]Wang L, Meng C G, Han M, et al. *J. Colloid Interface Sci.*, **2008**,**325**(1):31-40

[27]Naiya T K, Bhattacharya A K, Das S K. *J. Colloid Interface Sci.*, **2008**,**325**(1):48-56